

# A 2MASS All-Sky View of the Sagittarius Dwarf Galaxy: III. Constraints on the Flattening of the Galactic Halo

Kathryn V. Johnston<sup>1</sup>, David R. Law<sup>2,3</sup>, and Steven R. Majewski<sup>3</sup>

## ABSTRACT

M giants selected from the Two Micron All Sky Survey (2MASS) have been used to trace streams of tidal debris apparently associated with the Sagittarius dwarf spheroidal galaxy (Sgr) that entirely encircle the Galaxy. While the Sgr M giants are generally aligned with a single great circle on the sky, we measure a difference of  $10.4 \pm 2.6$  degrees between the mean orbital poles of the great circles that best fit debris leading and trailing Sgr, which can be attributed to the precession of Sgr's orbit over the range of phases explored by the data set. Simulations of the destruction of Sgr in potentials containing bulge, disk and halo components best reproduce this level of precession along the same range of orbital phases if the potential contours of the halo are only slightly flattened, with the ratio between the axis length perpendicular to and in the disk in the range  $q = 0.90 - 0.95$  (corresponding to isodensity contours with  $q_\rho \sim 0.83 - 0.92$ ). Oblate halos are strongly preferred over prolate ( $q_\rho > 1$ ) halos, and flattenings in the potential of  $q \leq 0.85$  ( $q_\rho \leq 0.75$ ) and  $q \geq 1.05$  ( $q_\rho \geq 1.1$ ) are ruled out at the  $3\text{-}\sigma$  level. More extreme values of  $q \leq 0.80$  ( $q_\rho \leq 0.6$ ) and  $q \geq 1.25$  ( $q_\rho \geq 1.6$ ) are ruled out at the  $7\text{-}\sigma$  and  $5\text{-}\sigma$  levels respectively. These constraints will improve as debris with larger separation in orbital phase can be found.

*Subject headings:* Sagittarius dwarf galaxy – Milky Way: halo – Milky Way: structure – Milky Way: dynamics – dark matter – Local Group

## 1. INTRODUCTION

Simulations of structure formation within the standard Cold Dark Matter cosmology predict that cluster-scale dark matter halos should typically be far from spherical, with

---

<sup>1</sup>Wesleyan University, Department of Astronomy, Middletown, CT (kvj@astro.wesleyan.edu)

<sup>2</sup>California Institute of Technology, Department of Astronomy, MS 105-24, Pasadena, CA 91125 (dr-law@astro.caltech.edu)

<sup>3</sup>Dept. of Astronomy, University of Virginia, Charlottesville, VA 22903-0818 (srm4n@virginia.edu)

shortest to longest axis ratios in density typically around  $(c/a)_\rho = 0.5$ , rarely greater than  $(c/a)_\rho = 0.8$ , and with no strong preference for oblate ( $q_\rho = (c/a)_\rho < 1$ ) or prolate ( $q_\rho = (a/c)_\rho > 1$ ) halos (Dubinski 1994; Jing & Suto 2002). Such studies have typically been limited to studying the shapes of halos on cluster-scales because the computational expense of resolving a large enough sample of galaxy-scale halos was prohibitive. Indeed, observations leading to estimates of  $(c/a)_\rho$  for a handful of external galaxies proved to be roughly consistent with these findings (see Merrifield 2002, Fig. 3 for a summary). More recently, preliminary analysis of *galaxy*-scale dark matter halos extracted from cosmological simulations predict that they could be systematically rounder than their larger counterparts, peaking around  $(c/a)_\rho = 0.65$  and with examples as round as  $(c/a)_\rho = 0.95$  (Bullock 2002; Flores et al 2004). This result is especially intriguing given at least one estimate for the shape of the Milky Way’s dark matter halo that suggests that it could indeed be rather spherical ( $(c/a)_\rho > 0.95$ , Ibata et al. 2001), placing it at the extreme of the extragalactic  $(c/a)_\rho$  range. However, this estimate was made using just a few dozen carbon stars thought to be associated with tidal debris from the Sagittarius (Sgr) dwarf galaxy because of their alignment with its orbit on the sky (velocity measurements and distance estimates could not conclusively support this association in most cases), and hence the accuracy of this measurement remains unclear.

Debris from the destruction of a satellite galaxy can provide a sensitive probe of deviations of the potential of the Milky Way from spherical symmetry. Such debris occupies orbits with a range of azimuthal time periods about the satellite’s own, and this leads to the phase mixing of debris ahead and behind the satellite along its orbit to form tidal tails (Johnston 1998). Helmi & White (1999) showed that in spherical potentials these tidal tails will gradually thicken within the orbital plane, due to the range of precession rates of turning points in debris orbits. In non-spherical potentials, the range in precession rates of the orbital poles will lead in addition to thickening of the debris perpendicular to the (instantaneous) orbital plane of the satellite. Hence, if the Milky Way is close to spherical, debris should always remain planar and appear close to a single great circle in the sky (Johnston, Hernquist, & Bolte 1996), but if the Milky Way is non-spherical the debris should, over time, spread to cover a significant fraction of the sky. Such an alignment of a sample of faint, high latitude carbon stars (Totten & Irwin 1998) along a single great circle on the sky previously led Ibata et al. (2001) to conclude  $(c/a)_\rho > 0.95$ .

More recently, Helmi (2004a) has cautioned that, since it can take a few orbits for debris to spread beyond its intrinsic thickness, stars released only a few orbits ago cannot be sensitive probes of potential flattening, and hence that none of the Sgr data sets thus far detected provide any significant constraint on  $q$ . In addition to Helmi’s (2004a) concern, the thickness of a debris stream will also increase with satellite mass. Hence, if either the

current mass or recent mass loss rate is poorly known these introduce additional uncertainties in trying to measure  $q$  from the thickness of a stream. As a final concern (and one that is much harder to correct for) thickening can also result from interactions with other massive — and possibly invisible — lumps in the halo (Moore et al. 1999; Ibata et al. 2002; Johnston, Spergel, & Haydn 2002).

In this paper we revisit the question of what constraint tidal tail stars associated with the Sgr dwarf can place on the flattening of the Galactic potential. Our approach differs significantly from previous work in that we use the orbit-alignment rather than thickening of the debris to measure the halo shape. For our analysis, we use M giants selected from the Two Micron All Sky Survey (Majewski et al, 2003 — hereafter Paper I). The Sgr M giants are thought to have ages of 2-3 Gyr (Paper I) and hence, the *thickness* of tidal streams constituted of these stars cannot be expected to provide a strong constraint on  $q$  (even ignoring the additional concerns about this method we raised above). However, the approximate distances estimated from the apparent magnitude of the M giants permit a clear separation between stars leading or trailing Sgr along its orbit (because continuous streams of debris can be traced directly back to the Sgr core) and, moreover, yield a detailed view of the three-dimensional configuration of these tidal tails (e.g., Paper I). As a consequence, rather than simply looking at the thickness of debris projected on the sky, we are able to measure the poles of the best-fit great circles (in two dimensions) or best-fit planes (in three dimensions) of the leading and trailing debris separately. We use the difference in orbital poles between the two debris trails to quantify the precession of the orbital plane over this range of orbital phase. The advantage of this powerful approach is that what we are measuring is sensitive to  $q$  alone — the thickness of the debris due to parent satellite mass, debris age, or scattering off of lumps in the halo potential do not have systematic effects in this signal and merely contribute to the uncertainty in our measurement.<sup>4</sup>

To determine the expected variation in orbital poles for different values of  $q_\rho$ , we run a series of N-body simulations that mimic the Sgr system as traced by M giants. We describe our numerical simulations in §2, compare them to the M giant data set in §3 and summarize our results and discuss future prospects for this approach in §4.

---

<sup>4</sup>It is conceivable that internal rotation of Sgr perpendicular to the orbital motion could lead to a systematic offset between the angular momentum distributions of the leading/trailing debris, mimicing orbital precession, but we do not consider this since no systematic rotation in Sgr’s core has been observed.

## 2. METHODS

Our simulation technique closely follows that outlined in Johnston, Hernquist, & Bolte (1996). The Milky Way is represented by a smooth, rigid potential, and Sgr by a collection of  $10^5$  self-gravitating particles whose mutual interactions are calculated using a self-consistent field code (Hernquist & Ostriker 1992).

As a starting point for our study we use the results of Law, Johnston, & Majewski (2004 — hereafter referred to as Paper IV; preliminary results were presented in Law et al. 2004), who perform simulations of satellite disruption along orbits that are consistent with Sgr’s current position, line-of-sight velocity and direction of motion tangential to the line-of-sight (deduced from the orientation of the M giant plane). The mass and amplitude of tangential motion ( $v_{\text{tan}}$ ) of Sgr and the potential of the Milky Way are systematically varied to find the closest possible fit (hereafter referred to as the default model) to the angular position, distance, and available line-of-sight velocity data for the 2MASS M giants along the leading/trailing streams. The default model is run in a three-component model for the Galactic potential, consisting of a Miyamoto-Nagai (1975) disk, Hernquist spheroid, and a logarithmic halo:

$$\Phi_{\text{disk}} = -\alpha \frac{GM_{\text{disk}}}{\sqrt{R^2 + (a + \sqrt{z^2 + b^2})^2}}, \quad (1)$$

$$\Phi_{\text{sphere}} = -\frac{GM_{\text{sphere}}}{r + c}, \quad (2)$$

$$\Phi_{\text{halo}} = v_{\text{halo}}^2 \ln(R^2 + (z^2/q^2) + d^2), \quad (3)$$

where  $\alpha = 1$ ,  $M_{\text{disk}} = 1.0 \times 10^{10} M_{\odot}$ ,  $M_{\text{sphere}} = 3.4 \times 10^{10} M_{\odot}$ ,  $v_{\text{halo}} = 114 \text{ km s}^{-1}$ ,  $a = 6.5 \text{ kpc}$ ,  $b = 0.26 \text{ kpc}$ ,  $c = 0.7 \text{ kpc}$ , and  $d = 12.0 \text{ kpc}$  and  $q = 1$  (i.e. the halo component is spherical in the default model). The distance of the Sun from the Galactic Center is taken to be  $R_{\odot} = 7 \text{ kpc}$ . Initially, the particles in the Sgr model are distributed according to a Plummer (1911) model

$$\Phi = -\frac{GM_{\text{Sgr},0}}{\sqrt{r^2 + r_0^2}}, \quad (4)$$

where  $M_{\text{Sgr},0} = 7.5 \times 10^8 M_{\odot}$  is the initial mass of Sgr and  $r_0 = 0.82 \text{ kpc}$  is its scale length. The satellite is allowed to evolve over five pericentric passages along an orbit with a pericenter of 14 kpc, an apocenter of 58 kpc, and a radial orbital time period of 0.9 Gyrs. (The exact extent of the orbit depends on the distance scale adopted for the M giants, which is currently set by assuming a 24 kpc heliocentric distance for the Sgr core.) At the point matching Sgr’s current position and line-of-sight velocity, the satellite in the default model has a bound mass of  $3 \times 10^8 M_{\odot}$ . In Paper IV we find that the data still allow some freedom in the exact form for the Galactic potential, but that within a given potential the final bound mass of

Sgr is constrained to within a factor of two, and, once this is known,  $v_{\text{tan}}$  can be found to within a few  $\text{km s}^{-1}$ .

Paper IV, in effect, finds the best-fitting set of parameters that describe the configuration of Sgr debris *projected onto* the instantaneous orbital plane, whereas the current discussion focuses on the variations in the position of the orbital plane itself. In this paper, we rerun Paper IV’s default model with a variety of halo flattenings ranging from  $q = 0.8$  to 1.45 (i.e., we consider both oblate and prolate potentials). Since we are interested in constraining the contours of the potential, we flatten these directly via parameter  $q$  in Equation (3) rather than generating them from a flattened density distribution. These oblate/prolate potentials correspond to even greater oblateness/prolateness (e.g. Fig. 1 in Helmi 2004a) of the isodensity contours in the effective distance range that Sgr’s orbit explores. Note that even our models with spherical halos have modestly flattened potential contours due to the contribution of the Galactic disk.

We recalculate the values of the Galactic halo scalelength  $d$  and  $v_{\text{tan}}$  for each value of  $q$  considered to obtain the best possible fit to the M giant distance and line-of-sight velocity data within each model of the Galactic potential (see Paper IV for a description of this fitting process). The calculated values for each choice of  $q$  are given in Table 1. Note that the orbital characteristics of the model dwarf will vary slightly for each of these models, and therefore the mass-loss history of the dwarf will depend on  $q$ . However, we do not revisit the question of the best-fit mass for Sgr in each of these potentials because we are only concerned with the differential precession of the poles of the tidal debris, which is independent of satellite mass.

Throughout the paper we deliberately compare the M giant data with our simulations as viewed from the Sun, despite the fact that orbital precession is most naturally discussed in reference to the Galactic Center. This is because transforming the data to a Galactocentric viewpoint would introduce distortions due to uncertainties in the distances to both the M giants and to the Galactic Center that might be confused with orbital precession. In contrast, our heliocentric viewpoint of the simulations is fixed by only requiring that our simulated Sgr has the correct current position and velocity relative to the Sun. Moreover, we prefer a heliocentric system because is the natural system for the Great Circle Cell Count analysis we perform in §3.2.

### 3. RESULTS

In §3.1 we present a qualitative assessment of Aitoff projections of Sgr debris, and demonstrate similarly to previous discussions (e.g. Helmi 2004a) that such qualitative analyses provide little information on halo flattening. In contrast, we adopt two quantitative approaches to assess the degree of orbital plane precession of the Sgr system. The first method (§3.2) relies on careful measurements of the mean great circle described by the  $(l, b)$  distributions of M giants in the leading and trailing tidal tails. As applied here, this method is virtually free of observational errors or errors in derived quantities, particularly the derived distances of the M giants. In the second method (§3.3) we analyze the orbital plane variation using the derived three dimensional distribution of the Sgr M giants. Both techniques advance previous discussions of the qualitative appearance of Sgr debris in Aitoff projections to show that a slightly oblate Milky Way potential is preferred.

#### 3.1. Aitoff Projections

Figure 1 shows the projection of the final positions of particles in the default simulation onto Sgr’s orbital plane, and demonstrates the  $\Lambda_{\odot}$  coordinate system of Paper I;  $\Lambda_{\odot}$  is the angular distance from Sgr along the plane of its orbit, defined to be zero at the core and increase in the trailing direction. The colors represent different debris “eras”, i.e. orbits (denoted as one apoGalacticon to the next apoGalacticon) on which the debris was stripped from the satellite — yellow for particles lost since apoGalacticon about 0.4 Gyr ago, magenta, cyan, and green for particles stripped from the dwarf two, three, and four orbits ago, respectively (the orbital period of Sgr in all of our model Galactic potentials is about 0.75-1.0 Gyr). In Paper IV we find that the positions and available velocities for Sgr M giants presented in Paper I are consistent with debris younger than about 1.9 Gyr (i.e. yellow, magenta or cyan) in these simulations. This age estimate is consistent with the expected 2-3 Gyr lifetimes of these stars — for the M giants to be a significant contributor to debris older than about 1.9 Gyr the stars would have to be stripped from the satellite less than one orbital period following their birth (see Paper I for a fuller discussion of this problem).

Figure 2 plots Aitoff projections of the final positions of particles in both spherical and moderately flattened halos ( $q = 1$  and  $q = 0.85$ ). Visual inspection of this figure confirms the Helmi (2004a) conjecture that *qualitative* differences in the apparent thickening or precession of the most recent debris (i.e. yellow, magenta, and cyan points) are fairly small over the range of potential flattenings shown, especially for younger debris. However, it is premature to conclude that these effects do not lead to measurable variations in the disposition of the Sgr debris. We now demonstrate that *orbital precession* of even the most recent Sgr debris

can be measured and used to discriminate between halo flattening models.

### 3.2. Great Circle Cell Orbital Poles

In their current configuration about the Milky Way, Sgr leading arm M giants predominate in the Northern Galactic Hemisphere while trailing debris M giants dominate the South. Paper I demonstrated (see their Fig. 6) clear differences in the location of the Sgr M giant Great Circle Cell Count (Johnston, Hernquist, & Bolte 1996) [“GC3”] peaks when the M giant sample is limited to  $b > +30^\circ$  versus  $b < -30^\circ$  subsamples, and suggested that the differences could relate to a combination of precessional and parallax differences between leading and trailing arm debris. We repeat the Paper I GC3 analysis on our simulations (using the yellow, magenta, and cyan debris that best represent the Paper I M giant data) to determine the degree of precessional shift as a function of  $q$ . Figure 3 compares the shape and positions of the GC3 peaks of the models to those of the M giant data, divided into  $b > +30^\circ$  (North/mostly leading arm) and  $b < -30^\circ$  (South/mostly trailing arm) subsamples. Other aspects of sample selection, including limiting to stars with distances between 13 and 65 kpc and ignoring the region around the Magellanic Clouds ( $260^\circ < l < 320^\circ$  and  $-53^\circ < b < -25^\circ$ ) were utilized to exactly match the selection criteria used to generate the GC3 plots in Paper I (their Fig. 6). The 13-65 kpc distance range limit serves to highlight the primary distance range for the debris corresponding to the yellow, magenta and cyan parts of the leading and trailing arms. For the observations, this limit also removes nearby disk M giants and more distant “M giants” at magnitudes where 2MASS photometry becomes less reliable, whereas for both the observations and the models it limits the effects of overlapping contaminating debris on each Sgr arm from extensions of the opposite Sgr arms. The shapes of GC3 peaks reflect departures from great circle symmetry *as viewed from the Sun*, while the size (e.g., FWHM) of the peak is a function of the debris width on the sky, convolved with the cell size (here adopted as a  $5^\circ$  wide cell<sup>5</sup>). The first thing to notice is the overall consistency of the simulated and actual M giant data in both the shape and size of the GC3 peaks for *both* hemispheres. The detailed matches are encouraging support for the conjecture that the simulations provide rather accurate representations of the actual Sgr M giant distribution.

The second thing to note is that while there is virtually no difference in the location

---

<sup>5</sup>Runs with narrower cell widths yield virtually identical peak locations and shapes to the results for  $5^\circ$  wide cells presented here, albeit with poorer signal-to-noise because of the fewer numbers of stars that fall within the narrower cells.

of the GC3 peaks for the southern (trailing arm) data as a function of  $q$ , the position of the GC3 peak for northern (leading arm) data is, in contrast, highly and systematically sensitive to  $q$ . The effect is more pronounced in the North because (a) the leading arm extends very close to (virtually on top of) the Sun and a given precessional shift relative to the Galactic center will be foreshortened to a larger angular shift on the sky for closer debris, and (b) the northern sample utilized includes a larger fraction of *older* debris, torn off from Sgr one orbit earlier (i.e., the cyan debris in Fig. 1), and these very stars, which will have experienced more precession, constitute much of the Sgr debris closest to the Sun in the North. Note that the simulations were not adjusted to create a best match to the GC3 poles in Figure 3, but rather the orbit of Sgr in the simulations was set by the mean pole ( $[l, b] = [273.75, -13.46]^\circ$ ) found in the Paper I single plane fit to the Cartesian positions of both leading and trailing M giant debris; the close match to the general positions of the separated North/South GC3 poles arises naturally from the evolution of the debris.<sup>6</sup> The poles in Figure 3 show the simulations with  $q = 0.90$  and  $q = 0.95$  to be the closest match to both the absolute positions of the northern hemisphere GC3 peak as well as the relative difference in North/South GC3 peak positions in the M giant data. More oblate and all prolate models yield northern GC3 peaks that are tens of degrees off from the observed positions. The GC3 analysis shows that subtle variation in the  $(l, b)$  distribution of debris (Fig. 2) *can* be measured and, in a way virtually free of observational bias, be used to constrain  $q_\rho$ .

### 3.3. Plane Fitting Poles

The GC3 analysis gives a phase-averaged view of the expected differential precession of Sgr leading and trailing debris. In contrast, the lines in Figure 4 show the pattern that the *instantaneous* pole of Sgr’s orbit traces on the sky within  $\pm 1.5$  Gyrs of Sgr’s current position, as viewed from the Sun. The upper/lower panels show the pole evolution in potentials with oblate/prolate halo components respectively, with the solid/dotted portions of each line corresponding to portions of the orbit trailing/leading Sgr. The black triangle shows the best fit pole of the 2MASS data set (Paper I), which the orbits were constrained to go through at Sgr’s current position.

The dots along each curve in Figure 4 indicate the pole position at 0.2 Gyr intervals both leading and trailing Sgr’s current location. The M giants discussed in Paper I explore

---

<sup>6</sup>Whereas a more precise match may be possible through trial and error adjustment of the instantaneous orbital pole of the Sgr core, this exact match is not essential to our goal of measuring *differences* between the leading and trailing debris.

orbital phases corresponding to up to (roughly) +0.6 Gyrs and -0.4 Gyrs from Sgr’s current position, ahead and behind it in time along the orbit. (Note that the debris age — i.e. the time since stars were lost from Sgr — is much greater than this.) Hence, the poles actually measured from the M giant and simulation data can be thought of as averages of 3 points along the dotted curves and 2 points along the solid curves, weighted by the density of stars or particles along the streamers. (Note that, for fixed flattening, the pole paths of orbits with  $v_{\text{tan}}$  varying from the adopted value by as much as  $\pm 10 \text{ km s}^{-1}$  — more than the maximum range permitted given constraints from the M-giant distances and velocities, as shown in Paper IV — were found to be virtually indistinguishable from the orbits illustrated.). This figure demonstrates (as already seen in Fig. 3) that: (i) In general, the separation of poles derived for the leading and trailing simulated data should increase with increasing deviations from  $q = 1$ ; (ii) pole separation should be more dramatic for the oblate cases than the prolate cases; (iii) the sense of precession in prolate potentials is opposite to that in oblate potentials; and (iv) some (oblate-like) precession should be present even in the  $q = 1$  case because of the presence of a disk component in our Galactic potential.

We might expect the lines in Figure 4 to move monotonically in Galactic longitude. The retrograde-looping evolution of the leading (dotted) portion in the oblate cases is due to our perspective of these orbits, which have pericenters that lie only just outside the Solar Circle. Indeed, some asymmetry between the evolution of the poles of leading and trailing debris is already apparent in the more dramatic shift of the GC3 peaks of the Northern (leading) debris when compared to the Southern (trailing), as noted in the previous section (Fig. 3). However, the Figure 3 GC3 analysis is a somewhat blunt tool for assessing the precessional shifts because it does not take advantage of all available information — namely, the distances to the stars/particles.

To quantify the degree of precession exhibited by Sgr debris better, the poles of best-fit orbital planes can be determined for both the M giant and the simulated data by plane-fitting to the leading and trailing arm debris in three-dimensional space. We constrain these planes to pass through the solar position to allow us to quantify the effect precession has on Sgr tidal debris as projected on the sky (the natural observational regime, e.g., as used in a GC3 analysis). This constraint means that the poles derived by this method should be interpreted only as tools for tracing the amount of precession in a given model of the Galactic potential; they are not the true Galactocentric orbital poles and do not precisely represent the angular momentum vector of the debris. The best-fit planes to the M giant and simulation distributions were found by minimizing the  $\chi^2$  distribution of point distances from the plane, applying an iterative 2.5- $\sigma$  rejection algorithm. Confidence limits on the corresponding poles were determined by statistical analysis of synthetic data sets generated using a bootstrapped Monte Carlo technique, with the confidence ellipse resulting from this

analysis projected into error bars at the 68% confidence level in  $l$  and  $b$ .

The open symbols in Figure 5 show the results of this precession analysis applied to data points in the leading tail in the range  $\Lambda_{\odot} = 220^{\circ} - 310^{\circ}$ , while the filled symbols show the results for the trailing tail in the range  $\Lambda_{\odot} = 20^{\circ} - 145^{\circ}$ <sup>7</sup> — see Figure 1. The colored triangles/squares correspond to simulated data run in prolate/oblate potentials. (The error bars on the simulated points are comparable to the symbol sizes and are omitted for clarity.) Note there is a systematic offset in  $(l, b)$  of order a few degrees between the results from the observed data and the trend of the simulated data. This can be attributed to our assumption that the pole derived from the full 2MASS data corresponds to Sgr’s present orbital pole when, in fact, it merely represents an average along tidal debris with a small range of orbital phases. Nevertheless it is clear that: (i) the *sense* of precession in the data strongly favors oblate potentials; and (ii) the evolution of pole *differences* in the plot implies that the precession rate is most consistent with our slightly flattened halo models in which  $q \approx 0.90$ . Table 1 emphasizes this result by quoting the separation of the leading/trailing poles for the simulations and the M giants. Flattenings within the range  $0.90 < q < 0.95$  ( $0.83 < q_p < 0.92$ ) lie within the  $1.5\text{-}\sigma$  error bars on the data, while those with  $q < 0.85$  and  $q > 1.05$  are ruled out at the  $3\text{-}\sigma$  level. More extreme values of  $q \leq 0.80$  ( $q_p \leq 0.6$ ) and  $q \geq 1.25$  ( $q_p \geq 1.6$ ) are ruled out at the  $7\text{-}\sigma$  and  $5\text{-}\sigma$  levels respectively.

The open/filled circles in the lower panel of Figure 5 show the results of the same analysis performed on the older (color coded green in Figs. 1 and 2) simulated data at larger separations along the orbit ( $\Lambda_{\odot} = 0^{\circ} - 120^{\circ}$  for the leading debris and  $200^{\circ} - 250^{\circ}$  for the trailing — see Fig. 1) for the  $q = 0.90$  simulation, which best reproduces the poles of the younger debris. The positions of the circles are suggestive of the evolution traced by the orbital poles in Figure 4. Note that the M giants discussed in Paper I are primarily in the yellow, magenta and cyan portions of the tidal debris (see Paper IV) and there is no clear evidence yet for M giants in the portions of the tails corresponding to the green debris; the phase-mixing time for debris to reach these points is comparable to the stellar evolution ages of these stars (see §3.1). The circles in Figure 5 demonstrate that an analysis such as that conducted here will provide a more powerful constraint on  $q$  if tracers of this older debris can be found, so long as leading debris, which will be mainly in the *Southern* Hemisphere for “green debris”, can clearly be separated from the *trailing* debris there using distance and/or

---

<sup>7</sup>These were selected as ranges in which Sgr tail M giants may readily be identified in the 2MASS database using the selection criteria  $E(B - V) < 0.555$ ,  $1.0 < J - K_s < 1.1$ ,  $|Z_{\text{Sgr}, \odot}| < 25$  kpc,  $|b| > 30^{\circ}$ , and distances  $13$  kpc  $< d_* < 60$  kpc. See Paper I for definitions of these criteria. The Magellanic Clouds were removed from this data set using the  $(l, b)$  cuts given in Paper I. For the simulations, yellow, magenta, and cyan debris were considered and subjected to the same cuts in  $\Lambda_{\odot}$ ,  $d_*$ , and  $b$  as the M giants.

velocity information. Indeed, at these larger phase-differences from Sgr, the leading/trailing poles differ by more than 45 degrees even for flattenings of  $q = 0.90$ . This suggests that the accurate determination of the centroid of an older piece of the Sgr tidal stream, even at a single longitudinal point, can provide strong leverage on  $q$  via comparison with test-particle integrations in different potentials.

#### 4. CONCLUSIONS AND FUTURE PROSPECTS

We have shown that the precession of Sgr’s orbit can be accurately traced by stars in its debris streams — even the relatively recently released M giant stars — and hence be used to constrain the flattening of the Galactic potential. A difference of  $10.4 \pm 2.6$  degrees is found between the best-fit orbital poles for stars in Sgr’s leading and trailing streams (in the sense that the angular momentum vector *increases* in  $l$  and *decreases* in  $b$  from trailing to leading debris) when those poles are measured from debris at azimuthal orbital phases within  $+140/-145$  degrees along its orbit as viewed from the Sun. Such a low amount of precession is most consistent (within  $1.5\text{-}\sigma$ ) with simulations of the destruction of Sgr run in models of the Galaxy with a slightly flattened halo where  $q$  is in the range  $0.90 - 0.95$  ( $q_\rho = 0.83 - 0.92$ ). Flattenings for the halo potential of  $q = 0.85$  ( $q_\rho = 0.75$ ) or less and  $q = 1.05$  ( $q_\rho = 1.1$ ) or more are ruled out at the  $3\text{-}\sigma$  level, and oblate models are strongly preferred over prolate models. Note that these results depend on the assumed form of the potential of the Galactic disk.

Recently, Helmi (2004b) has suggested that prolate Milky Way potentials offer a means by which to solve a dilemma discussed in Paper IV — namely that the Sgr leading arm radial velocities are one discrepant observable not well fit by oblate Milky Way + Sgr models that provide compelling overall fits to all other available observables (see Paper IV). While a prolate model solves this one problem, as shown here prolate models also introduce a serious discordance with the observed M giant precession; indeed, prolate models are found to induce precession in the *opposite* direction to that observed. Since orbital pole precession is almost solely sensitive to the shape of the potential, whereas a variety of other effects in addition to the halo shape — e.g., evolution in the Sgr orbit and/or the strength of the Galactic potential — can conceivably alter the dynamics of debris *within* the orbital plane, we are inclined to the simpler explanation of an oblate potential to match the precessional data while admitting the need for yet more sophisticated models to resolve the problem with the leading arm velocities using these other free parameters.

Future detections of older Sgr debris at larger phase-differences along its orbit will provide even stronger orbital precession constraints than obtained here. Recently, Newberg

et al. (2003) announced a new detection of Sgr debris as an over-density of A-colored stars in the Sloan Digital Sky Survey at sufficient angular separation from Sgr ( $\Lambda_{\odot} \sim 196^{\circ}$ ) and distance from the Sun ( $> 80$ ) kpc to possibly associate it with the oldest (green) debris in our simulations. Unfortunately, the debris has not yet been mapped fully enough for a determination of its mean position; when done, however, a more accurate determination of  $q$  may be possible. Thus, Sgr has still more to contribute to our understanding of the Galactic potential.

SRM acknowledges support from a Space Interferometry Mission Key Project grant, NASA/JPL contract 1228235, NSF grant AST-0307851, a David and Lucile Packard Foundation Fellowship, and the F.H. Levinson Fund of the Peninsula Community Foundation. KVJ's contribution was supported through NASA grant NAG5-9064 and NSF CAREER award AST-0133617.

## REFERENCES

- Bullock, J. S. 2002, in *The Shapes of Galaxies and Their Dark Halos*, ed. P. Natarajan, (Singapore: World Scientific), p.109
- Dubinski, J. 1994, *ApJ*, 431, 617
- Flores, Bullock, J. , Kravtsov, A., Allgood, & Primack, J. 2004, in preparation
- Helmi, A. & White, S. D. M. 1999, *MNRAS*, 307, 495
- Helmi, A. 2004a, *MNRAS*, 351, 643
- Helmi, A. 2004b, *ApJ*, 610L, 97
- Hernquist, L. & Ostriker, J.P. 1992, *ApJ*, 386, 375
- Ibata, R. A., Lewis, G. F., Irwin, M. J., & Quinn, T. 2002, *MNRAS*, 332, 915
- Ibata, R.A., Lewis, G. F., Irwin, M.J., Totten, E., & Quinn, T 2001, *ApJ*, 551, 294
- Jing, Y. P. & Suto, Y. 2002, *ApJ*, 574, 538
- Johnston, K. V., Spergel, D. N., & Haydn, C. 2002, *ApJ*, 570, 656
- Johnston, K.V. 1998, *ApJ*, 495, 297
- Johnston, K. V., Hernquist, L., & Bolte, M. 1996, *ApJ*, 465, 278

- Law, D. R., Majewski, S. R., Johnston, K. V., & Skrutskie, M. F. 2004, in *Satellites and Tidal Streams*, eds. F. Prada, D. Martinez-Delgado, T. Mahoney, ASP Conf. Ser., *in press* (astro-ph/0309567)
- Law, D.R., Johnston, K.V., & Majewski, S.R. 2004, *ApJ*, submitted. (“Paper IV”)
- Majewski, S. R., Skrutskie, M.F., Weinberg, M.D. & Ostheimer, J.C. 2003, *ApJ*, 599, 1082. (“Paper I”)
- Merrifield, M. R. 2002, in *The Shapes of Galaxies and Their Dark Matter Halos*, ed. P. Natarajan, (Singapore: World Scientific), p.170
- Miyamoto, M. & Nagai, R. 1975, *PASJ*, 27, 533
- Moore, B., Ghigna, S., Governato, F., Lake, G., Quinn, T., Stadel, J., & Tozzi, P. 1999, *ApJ*, 524, L19
- Newberg, H. J. et al. 2003, *ApJ*, 596, 191
- Plummer, H.C. 1911, *MNRAS*, 71, 460
- Totten, E.J. & Irwin, M.J. 1998, *MNRAS*, 294, 1

$q$	$d$ (kpc)	$v_{\text{tan}}$ (km s <sup>-1</sup> )	Pole Separation (degrees)
Sgr M giants			10.4 ± 2.6
0.80	13	286	32.7 ± 0.5
0.85	13	284	17.2 ± 0.5
0.90	13	280	11.5 ± 0.5
0.95	12	272	6.3 ± 0.5
1.00	12	270	3.3 ± 0.5
1.05	12	268	1.2 ± 0.4
1.10	12	264	0.5 ± 0.5
1.15	12	262	-2.2 ± 0.4
1.20	11	256	-2.5 ± 0.4
1.25	11	254	-2.9 ± 0.4
1.30	11	252	-2.9 ± 0.4
1.35	11	250	-3.9 ± 0.4
1.40	11	250	-4.1 ± 0.5
1.45	11	250	-5.0 ± 0.4

Table 1: Orbital pole precession of tidal debris between  $20^\circ < \Lambda_\odot < 145^\circ$  (trailing debris) and  $200^\circ < \Lambda_\odot < 320^\circ$  (leading debris) for Sgr M giants and simulations with indicated values of the Galactic halo flattening  $q$ . Positive separation values indicate simulations whose leading debris orbital pole is at higher/lower  $l/b$  than the trailing debris pole, and negative values indicate simulations whose leading debris pole is at lower/higher  $l/b$  than the trailing debris pole (i.e. in the direction opposite to that observed for Sgr M giants, see Fig. 5). The values assumed for the halo scale length ( $d$ ) and the velocity of the model dwarf tangential to the line of sight ( $v_{\text{tan}}$ ) in each model are also given.

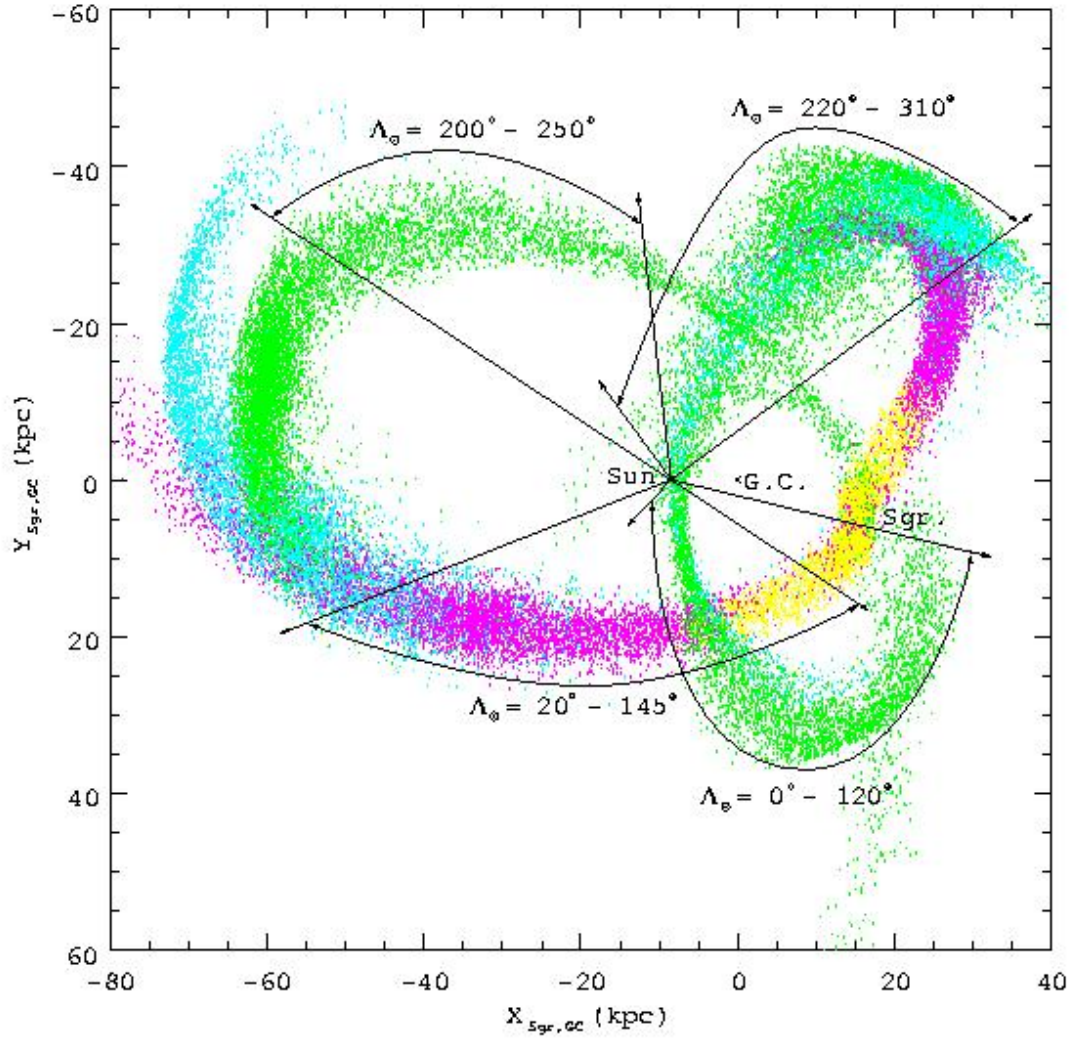


Fig. 1.— Appearance of a typical model of Sgr tidal destruction (from Paper IV) in the Sgr plane coordinate system (see Paper I). The location of the Sun, Galactic Center and Sgr dwarf are marked. Yellow particles became unbound from the dwarf since the last Sgr apoGalacticon (about 0.4 Gyr ago), and particles lost in successive preceding orbits are coded as magenta, cyan and green points. Labels indicate regions of debris used for precession analysis in Section 3.3.

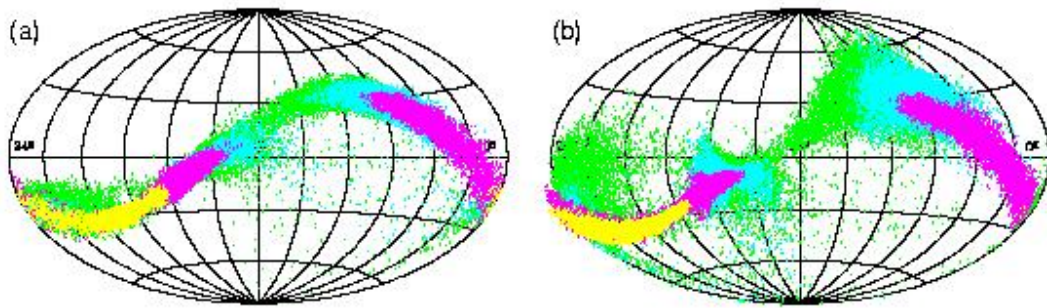


Fig. 2.— Aitoff projections of debris particles in our simulations with (a)  $q = 1$  and (b)  $q = 0.85$ , with the same color coding as Figure 1.

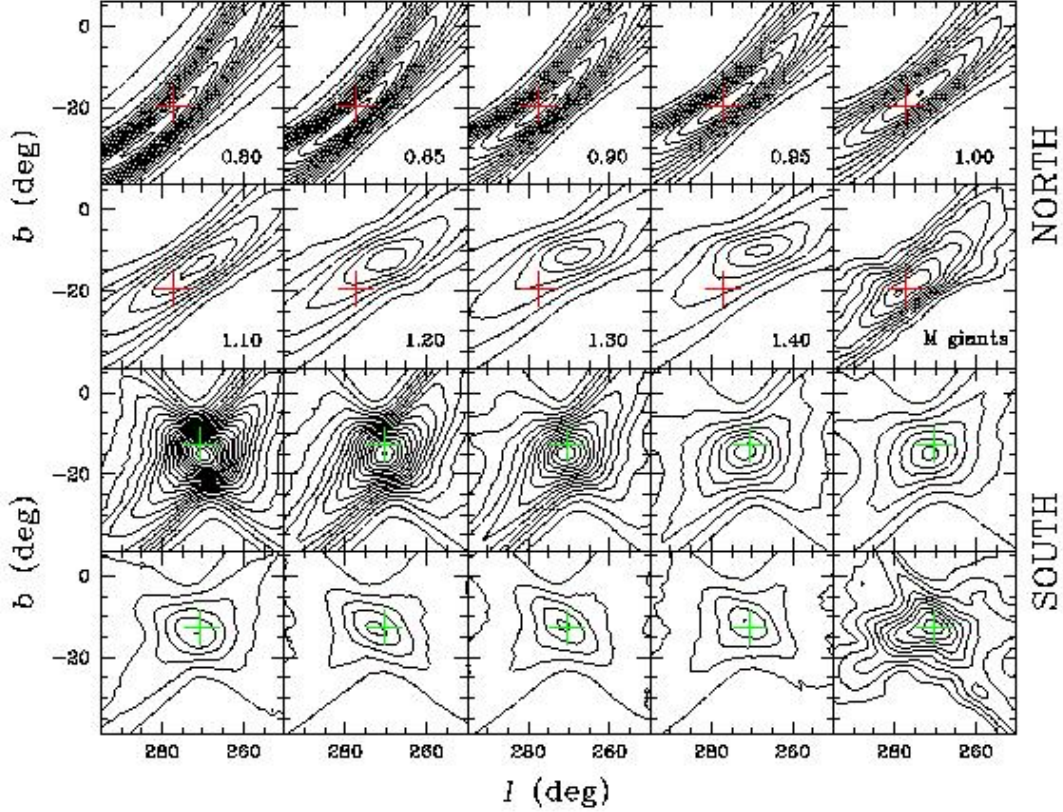


Fig. 3.— Close-up views of the GC3 peaks corresponding to Sgr debris in simulations with varying  $q$  parameters as well as to the actual M giant data. The M giant data shown are exactly those in Figure 6 of Paper I. The upper two rows show the peaks derived from GC3 analysis of all simulation particles or M giants with  $b > +30^\circ$  while the bottom two rows correspond to simulations/data with  $b < -30^\circ$ . The  $q$  values shown in the panels in the upper rows are not repeated in the bottom panels (for clarity), but map identically from the upper ten to the lower ten panels. The contour levels have linear spacing, separated in steps of 400 for the North simulations, 150 for the South simulations, and 20 for the actual M giant data. The resolution of the GC3 maps is 1 degree in both  $l$  and  $b$ , while the cell size for the maps shown are  $5^\circ$ . The cross symbols are North (red) and South (green) reference guides, set to the approximate centers of the peaks in the North and South M giant data respectively, and are repeated in the same locations across the maps for the corresponding simulations. A clear shifting of the orbital pole positions with  $q$  is evident in the Northern Hemisphere (leading arm), but to a much less extent in the Southern Hemisphere (trailing arm). The simulations that match the M giant data closest are those with  $q = 0.90$  and  $q = 0.95$ .

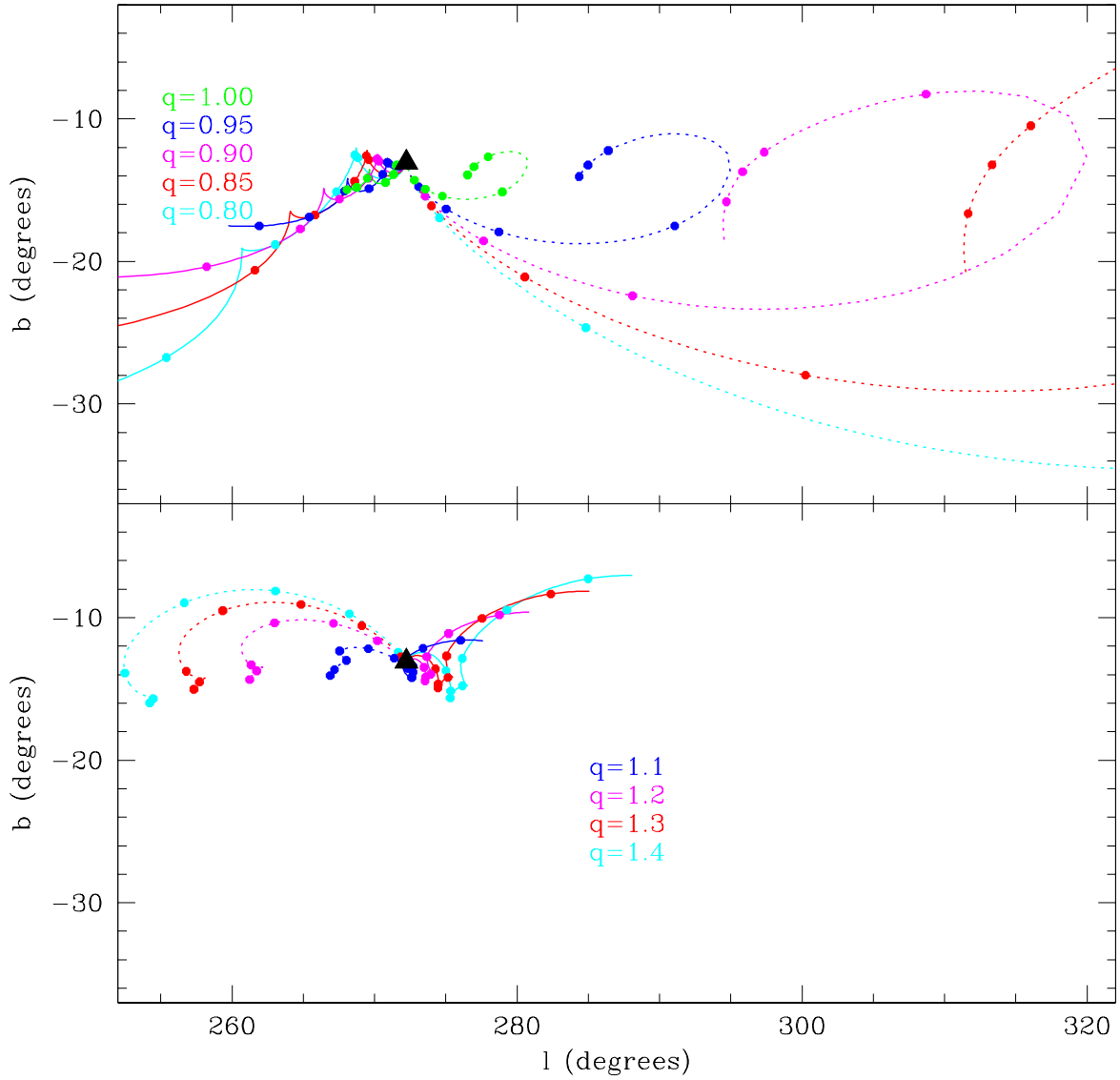


Fig. 4.— The evolution of Sgr’s instantaneous orbital pole  $\pm 1.5$  Gyrs along its orbit in potentials with  $q \leq 1$  (top panel) and  $q > 1$  (bottom panel). The *black triangle* shows the pole calculated from the combined leading and trailing M giant debris. Tickmarks on each evolutionary path represent time intervals of 0.2 Gyrs and the solid/dotted lines indicate trailing/leading portions (see text).

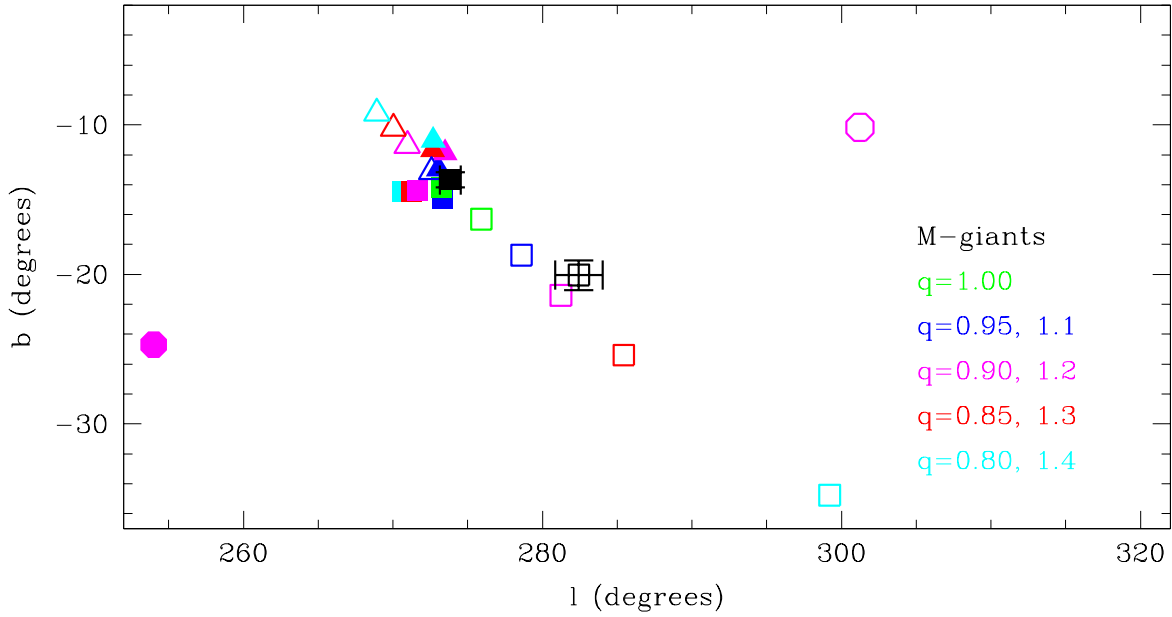


Fig. 5.— The positions of apparent orbital poles for the M giants and simulated debris calculated using the plane-fitting technique. Open/filled symbols represent the poles of leading/trailing debris, Squares/triangles are for oblate/prolate potentials. Circles represent orbital poles for the  $q = 0.90$  simulation calculated from older, more greatly precessed tidal debris.